Journal of Materials Chemistry C

RSCPublishing

ARTICLE

Size controlled synthesis of carbon quantum dots using hydride reducing agents†

Cite this: DOI: 10.1039/x0xx00000x

Keith Linehan and Hugh Doyle*

Received 00th January 2012,
Accepted 00th January 2012

DOI: 10.1039/x0xx00000x

www.rsc.org/

Highly luminescent carbon quantum dots (CQDs) are synthesized at room temperature by hydride reduction of carbon tetrachloride (CCl_4) within inverse micelles. Regulation of the average diameter of the allylamine terminated CQDs is achieved by varying the strength of the reducing agent used. Transmission electron microscopy shows that the NCs are highly crystalline with well-defined core diameters tuned from 2 to 6 nm, while FTIR and XPS spectroscopy confirm that the CQDs possess similar surface chemistry. UV-Vis and PL spectroscopy show significant quantum confinement effects, with moderate absorption in the UV spectral range, and a strong, narrow luminescence in the visible with a marked dependency on excitation wavelength. Time resolved photoluminescence measurements showed lifetimes for all CQDs in the ns range, while a maximum PL quantum yield of 27% is observed for the CQDs.

Introduction

Over the last few years luminescent carbon quantum dots (CQDs) have received widespread interest owing to their attractive photophysical properties, high quantum yields, low toxicity and biocompatibility.[1-3] Compared to conventional organic dyes and semiconductor quantum dots, CQDs possess advantages in terms of chemical inertness, easy functionalisation, high resistance to photobleaching,[4-7] an absence of fluorescence intermittency[1,4] and the potential for low cost production. Despite the great potential of this material, size and shape control for CQDs remains less developed than those for II-VI, IV-VI and III-V semiconductors. The ability to control the size and tailor the surface chemistry of the CQDs would facilitate in the understanding of size dependent phenomena and quantum confinement behaviour.[1,3] Biological applications such as bio sensing and cell imaging require tuning the optoelectronic and surface properties, thus controlling the shape and size distributions is of the utmost importance. Moreover, for carbon quantum dots to be used effectively in many biological applications, it is essential that they are water-soluble and stable against aggregation and precipitation within a biological system, possess a high photoluminescence quantum yield in the visible region and excellent photostability.[1,3,8]

A number of different synthetic strategies have been developed and reported for the preparation of CQDs, which may be divided into physical and chemical methods. Physical methods include arc discharge,[9] laser ablation/passivation[4, 10] and plasma treatment.[11] Chemical methods include electrochemical synthesis,[12-14] combustion and acidic oxidation,[15,16] hydrothermal and pyrolysis routes,[17] supported synthesis[18-20] and microwave/ultrasonic synthesis.[21,22] However, some drawbacks associated these methods include extensive post-synthetic purification, lack of control of CQD surface chemistry and sample polydispersity. To date very few reports exists for simultaneously controlling the size and tailoring the surface chemistry of the CQDs. Kang and co-workers developed a current density controlled electrochemical method to control the size of the CQDs, however the size distribution of the CQDs remained broad.[23] Jana and co-workers developed a chemical method to synthesis highly fluorescent carbon nanoparticles which exhibited size dependent and tunable emission in the visible region.[8]

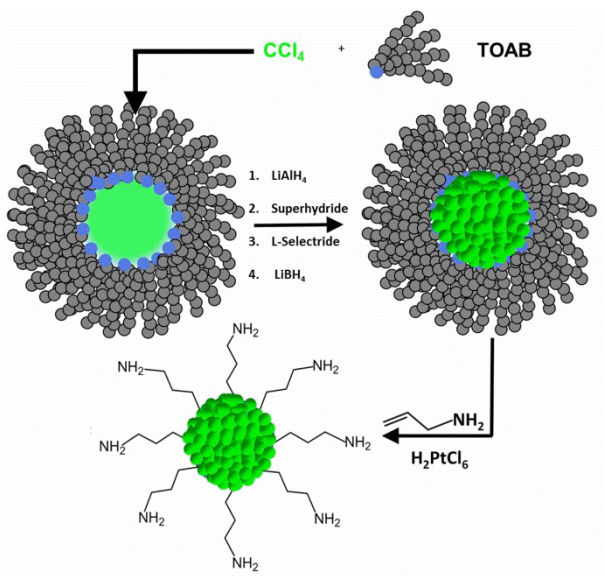

Fig. 1. Reaction scheme for the synthesis of carbon quantum dots.

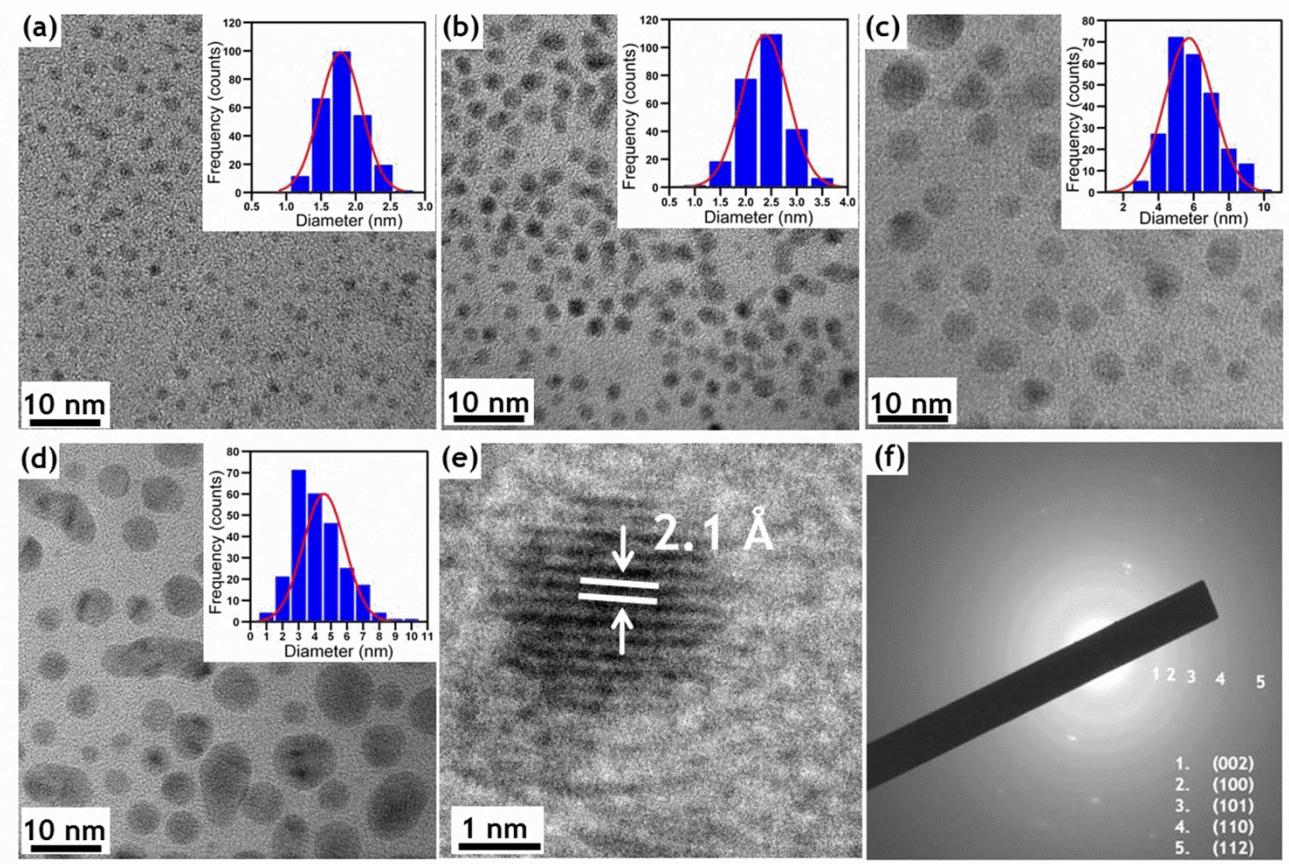

Fig. 2. Representative TEM images of the CQDs synthesized in the presence of the following hydride reducing agents: a) $LiAlH_4$, b) $Li(C_2H_5)_3BH$, c) $Li(CH(CH_3)CH_2CH_3)_3BH$, and d) $LiBH_4$. Inset: Size histograms of the CQDs with curves fit to the data using a Gaussian model. e) HR-TEM and f) SAED pattern, of the Carbon quantum dots synthesized using $Li(C_2H_5)_3BH$ as the reducing agent.

Whilst some of these methods have had some varying degree of success at controlling the size, key aspects such as tailoring the surface chemistry still needs to be improved. The use of microemulsion based synthetic methods have been the most promising due to their ability to control the size, shape and surface chemistry of CQDs. Rhee and co-workers reported the solution-phase synthesis of CQDs using reverse micelles as nanoscale reactors via condensation polymerisation and subsequent carbonization of glucose within AOT micelles at 160 ºC.[24] Control of the water-surfactant ratio within the micelle allowed the CQD diameter to be tuned from 1.8 to 4.1 nm, but with increasing polydispersity at larger diameters. More recently, Rhee *et al.* reported the synthesis of size tunable CQDs using a soft template method.[25] The size of the CQDs was controlled by regulating the amount of the emulsifier.

Previously, we reported the synthesis of size monodisperse CQDs using a room temperature microemulsion strategy,[7,26] see Fig. 1. The surfaces are terminated with a covalently attached amine monolayer, rendering the resulting hydrophilic quantum dots dispersible in a wide range of polar solvents. Solution phase reduction synthesis employing microemulsion methods for the preparation CQDs have been limited and to the best of our knowledge, no detailed studies have been carried out on the effect of hydride reducing agents in controlling the size and shape of the resultant CQDs. With this in mind, our aim was to develop a synthetic method that permits both control over the size, shape and surface, and allows for the high crystallinity and monodispersity within the material. Here we report a simple room temperature method for the size controlled synthesis of CQDs within inverse micelles having well defined core diameters ranging from 2 to 6 nm. The CQDs are chemically passivated and made water soluble using an allylamine ligand. Regulation of the CQDs size was achieved by utilizing hydride reducing agents of different strengths. Through controlling the size of the CQDs, their resulting photoluminescence properties could be tuned.

Results and discussion

Amine-terminated CQDs were synthesized by room temperature reduction of carbon tetrachloride under inert atmosphere conditions; see Experimental Section and Fig. 1 for further details. In this study, hydride reducing agents of different reactivities are compared. Lithium aluminium hydride ($LiAlH_4$), is the strongest reducing agent followed by lithium triethylborohydride (Superhydride®, $Li(C_2H_5)_3BH$), lithium tri-

sec-butylborohydride (L-Selectride®, $Li(CH(CH_3)CH_2CH_3)_3BH$) and lithium borohydride ($LiBH_4$). Fig. 2 shows low magnification transmission electron microscope (TEM) images of CQDs prepared in the presence of the different hydride reducing agents. TEM imaging of CQDs synthesized in the presence of the strongest reducing agent $LiAlH_4$ (Fig. 2(a)) show that the CQDs are highly size and shape monodisperse, with no evidence of aggregation. Inset in Fig. 2(a) is a histogram of CQD diameters, determined by analysis of TEM images of 250 CQDs located at random locations on the grid. Fitting the histogram to a Gaussian model yielded a mean diameter of 1.8 nm, with a standard deviation of 0.3 nm, closely matching with the (002) interplanar spacing of graphite, emphasizing the highly size monodisperse nature of the CQD. Fig. 2(b) shows a low resolution TEM image of CQDs prepared using Superhydride as the reducing agent. The CQDs were again found to be predominantly monodisperse and spherical with a mean diameter 2.1 ± 0.4 nm. Replacing superhydride with either L-Selectride or $LiBH_4$ resulted in an increase in the mean CQD diameter to 4.5 ± 1.5 nm and 5.5 ± 1.4 nm respectively, see Fig. 2(c) and 2(d). Whilst the mean CQD diameter increased using L-Selectride, the shape of the CQDs remained spherical, however the CQDs prepared by the reduction using $LiBH_4$ were found to be larger in size, accompanied by a significant increase in size polydispersity and more irregular in shape, see also Fig. S1 of the ESI.

Lithium aluminium hydride is the most powerful reducing agent used in this work due to the weaker bond strength of Al-H compared to B-H. As a result, the reaction occurs rapidly and there is rapid consumption of the CCl_4 precursor during the initial nucleation phase, leaving little precursor material available for subsequent growth in solution. A similar trend is observed for the reduction by Superhydride, leading to formation of smaller and more monodisperse quantum dots. However the CQDs formed by the weaker reducing agents L-Selectride or $LiBH_4$ resulted in larger sizes which may be due to less precursor consumption during the initial nucleation burst, and as a result, more unreacted CCl_4 is available for subsequent CQD growth. High-resolution TEM (HR-TEM) imaging was used in conjugation with selective area diffraction (SAED) to confirm the crystallinity and establish the crystal phase of the as-synthesized CQDs; see Fig. 2(e-f) and Fig. S2 of the ESI. HR-TEM imaging of CQDs produced using Superhydride (Fig. 2(e)) as the reducing agent showed that the CQDs formed a single contiguous crystalline phase, without the presence of packing defects. The lattice fringes shown in Fig. 2(e) correspond to a *d* spacing of 2.1 Å, matching the (100) spacing reported for the graphite unit cell. The selected area diffraction (SAED) in Fig. 2(f), exhibited diffraction rings that could be indexed to the (002), (100), (101), (110) and (112) planes.

The surface chemistry of the CQDs was investigated using high resolution XPS and FTIR spectroscopy, see Fig. 3. The C1s spectrum in Fig. 3(a) has a strong peak at 284.8 eV, assigned to C-C/C-H bonding, and two minor peaks at 286.2 and 287.8 eV are assigned to C-N and C-O bonding, respectively. The O1s spectrum in Fig. 3(b) has a single peak at 531.9 eV, assigned to the presence of C–Ox groups at the CQD surface. The N1s spectrum presented in Fig. 3(c) is fitted with two components at 399.3 and 401.1 eV, assigned to C-N and N-H bonds, respectively.

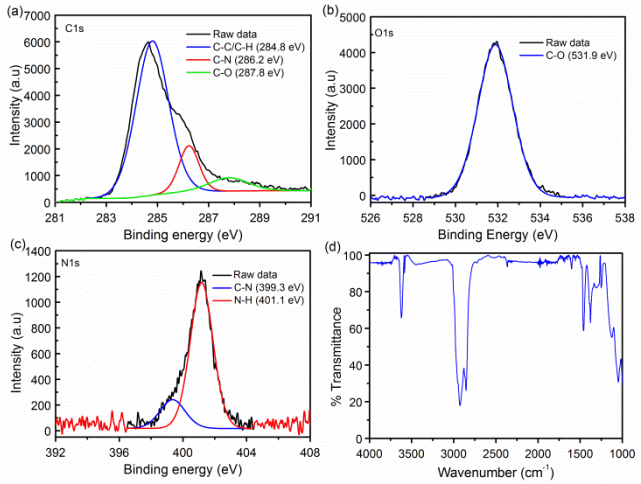

Fig. 3. (a-c) XPS and (d) FTIR spectra of allylamine terminated CQDs.

Fig. 3(d) shows the FTIR spectra of the allylamine-terminated CQDs. The peaks between *ca.* 3700- 3500 cm^{-1} are assigned to the N-H stretching of the amine, while the peaks observed between 3000-2850 cm^{-1} are attributed to C-H stretching modes. The feature centred near 1670 cm^{-1} is consistent with amine N-H deformation modes, but also with stretching modes of carboxylate species caused by surface oxidation, consistent with the XPS results. The peaks observed from 1500 - 1400 cm^{-1} are attributed to C-C bending modes. The absence of the characteristic $CH=CH_2$ peaks at 1640 and 3080 cm^{-1}, is consistent with successful binding of the allylamine ligand to the CQD surface, as previously reported.[7] Additional peaks below 1300 cm^{-1} are probably due to the presence of adventitious oxygenic surface species, in agreement with XPS characterisation results.

Fig. 4(a) shows the UV-Vis absorption spectra of the CQDs in water prepared using the different hydride reducing agents. The spectrum of the smallest nanocrystals (1.8 nm), synthesized when $LiAlH_4$ was employed as reducing agent, showed a broad absorption band centred at *ca.* 270 nm with an onset of absorbance located at 480 nm. This is in excellent agreement with our previous reports for similarly sized amine-terminated CQDs.[7] Increasing the mean quantum dot diameter using Superhydride or L-Selectride as the hydride reducing agent resulted in a distinct red-shift in the wavelength position of the absorption band to 304 and 306 nm, respectively. A further red shift in the absorption spectrum was observed when $LiBH_4$ was employed as the reducing agent, showing a strong peak centred at 315 nm, corresponding to a 45 nm shift compared to the smallest (1.8 nm) nanocrystals. Interestingly, the changes in CQD size do not significantly affect the onset of absorbance, located at *ca.* 480 nm (3.2 eV).

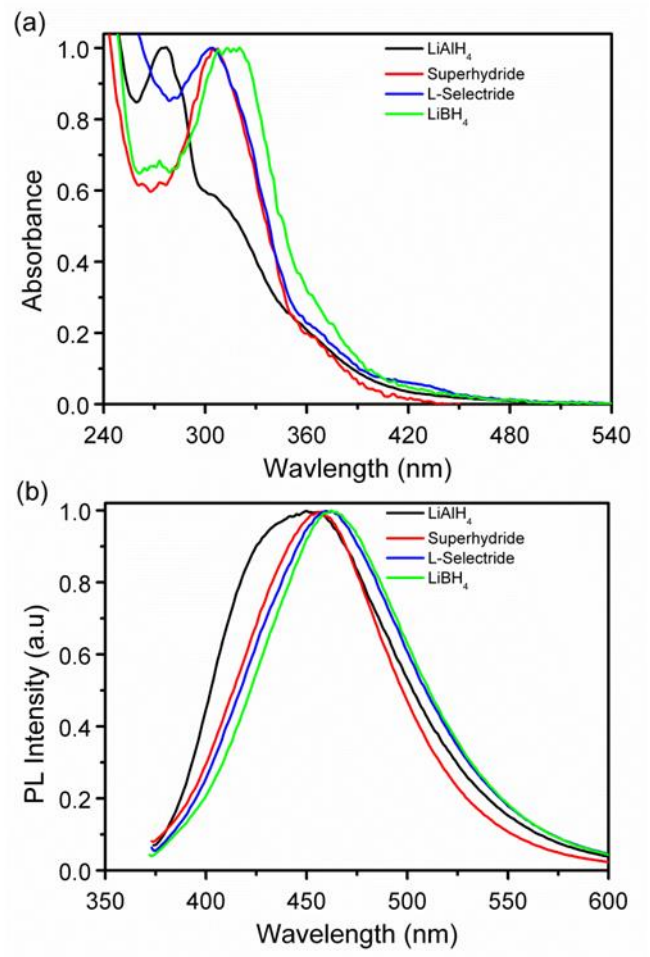

Fig. 4. (a) Normalised UV-Vis absorption spectra (b) Photoluminescence spectra of the CQDs.

Fig. 4(b) shows normalized photoluminescence spectra (360 nm excitation) of dilute dispersions of the CQDs in water, prepared with the same optical densities for comparison. Luminescence from the CQDs is observed over a narrow spectral range, with relatively little change as the diameter of the CQDs increases. For the smallest size CQDs the PL maximum emission was found to be at 450 nm, red-shifting with increasing quantum dot size, with the largest quantum dots showing a maximum emission at 462 nm. All the CQDs in this study showed a clear dependence on the excitation wavelength used, with the wavelength position of the PL maximum red-shifting as the excitation wavelength is increased from 300 nm to 440 nm, see Fig. S3 of the ESI. This is in good agreement with literature reports for CQDs dispersed in water.[11, 20]

The exact origin of PL from CQDs remains a contentious topic: the wide variety of synthetic strategies reported, together with broad particle size distributions, different ligand passivation schemes and varying degrees of oxidation have all contributed to the lack of consensus.[1, 3] Interestingly, in all reports the PL spectra of CQDs exhibit a clear excitation wavelength dependence for the emission maximum and intensity, which has been attributed to differently sized nanoparticles, different emissive trap states at the carbon dot surface, or other unresolved mechanisms.[1] Although the photophysical properties of CQDs have been demonstrated to depend on nanocrystal size, since graphitic carbon is not a semiconductor,[2] it is problematic to explain this using the bandgap exciton recombination description used for semiconductor QDs. Sun *et al.* attributed the PL from CQDs to the presence of surface energy traps that become emissive upon surface passivation.[4] They noted that this requirement was shared by CQDs and Si NCs, but that a large surface-to-volume ratio is required in order for the nanocrystal to exhibit strong photoluminescence upon surface passivation.

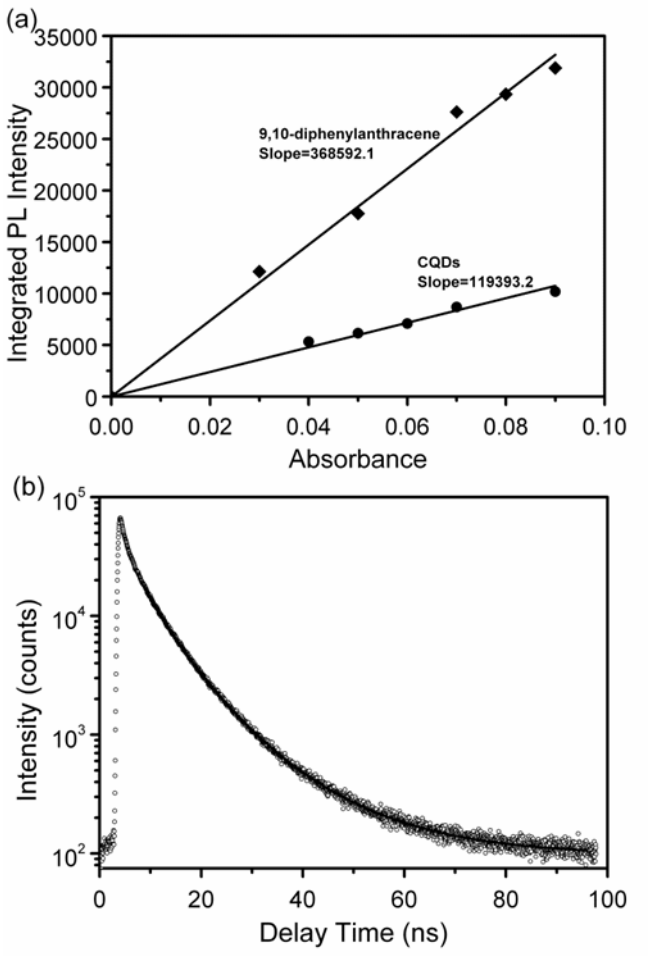

Fig. 5. Integrated PL intensity versus absorbance for an aqueous CQD dispersion and a solution of 9,10-diphenylanthracene in cyclohexane. (b) PL decay of the allylamine capped CQDs.

We have recently demonstrated that similar sized CQDs exhibit distinctly different absorbance and photoluminescence spectra when capped with ligands of different polarity, underlining the importance of the surface in determining their photophysical properties.[7, 26] Due to the high degree of monodispersity within those samples, we concluded the most plausible explanation was that the excitation wavelength dependence observed originated from recombination of photogenerated excitons at different surface trap states.

Table 1. Table of quantum yields measured in solution with fitted time constants and relative amplitudes determined from PL transients.

Reducing agent	Quantum yield	A1 (%)	τ1 (ns)	A2 (%)	τ2 (ns)	A3 (%)	τ3 (ns)	χ^2
$LiAlH_4$	27.1	26	3.1 ± 0.1	63	6.7 ± 0.1	11	15.8 ± 0.2	1.24
Superhydride	24.6	6	0.5 ± 0.4	61	4.5 ± 0.1	33	11.8 ± 0.1	1.10
L-Selectride	18.4	26	1.6 ± 0.1	59	5.6 ± 0.1	15	13.0 ± 0.1	1.20
$LiBH_4$	19.4	15	2.6 ± 0.2	63	6.3 ± 0.1	22	13.0 ± 0.1	1.26

Since the surface of the CQDs were capped using the same ligand functionalisation method, any variation in the PL spectra shown in Fig. 4(b) would be due to size effects, although the increased polydispersity of the larger CQDs would also have some contribution. The similarly of the PL spectra for different sized CQDs observed supports the interpretation that the PL mechanism is dominated by surface trap states.[27] The relative photoluminescence of the CQDs was shown to increase with decreasing diameter (and thus, increasing surface-to-volume ratio), in agreement with reports by Sun *et al.*[4]

Fig 5(a) shows the integrated PL intensity of dilute dispersions of 1.8 nm diameter CQDs in water compared to the emission standard used, 9,10-diphenylanthracene in cyclohexane. Linear regression analysis was employed to determine the relative PL intensities of the sample and reference solutions over the range of concentrations; see Fig. 4 of the ESI for additional plots and analyses of the CQDs synthesised using the other reducing agents. When $LiAlH_4$ was used as the reducing agent, the quantum yield was found to be *ca.* 27% at an excitation wavelength of 320 nm, comparable to values obtained for CQDs reported in the literature. As discussed above, the quantum yields generally decrease with increasing quantum dot diameter, with the largest size quantum dots exhibiting a quantum yield of 19.3%, see Table 1.

Further insight into the photophysical behaviour of the CQDs was obtained using time-resolved photoluminescence spectroscopy. Photoluminescence transients of the CQDs were acquired using time-correlated single photon counting methods (λ_{ex} = 402 nm); see Fig. 5(b). Measured transients were well fitted to the sum of three weighted exponentials; the fitted time constants and relative amplitudes are summarised in Table 1. From Table 1, it can be seen that the dominant lifetime component is between 4.5 - 6.7 ns, while other contributions with time constants of 1 - 3 ns and 12 - 16 ns are also present in the PL transients.

Experimental

Carbon Quantum Dot Synthesis

Carbon tetrachloride (≥ 99.5 %, anhydrous), chloroplatinic acid (≥ 99.9 %), lithium aluminium hydride (1.0 M in THF), Superhydride® (1.0 M in THF), L-Selectride® (1.0 M in THF), lithium borohydride (2.0 M in THF), allylamine (≥ 99 %), toluene (99.8 %, anhydrous), methanol (99.8 %, anhydrous) and isopropyl alcohol (99.5 %, anhydrous) were purchased from Sigma Aldrich Ltd. and stored under inert atmosphere before use. Tetraoctylammonium bromide (98 %), 9,10-diphenylanthracene (97 %), cyclohexane (≥ 99.9 %), sulphuric acid (95-97 %) and hydrogen peroxide (30% v/v) were purchased from Sigma Aldrich Ltd. and stored under ambient atmosphere. All reagents and solvents were used as received. In an inert atmosphere glove-box, 3.2 g (5.94 mmol) of tetraoctylammonium bromide (TOAB) was dissolved in 100 mL anhydrous toluene. 0.2 mL (2.06 mmol) CCl_4 was then added to the solution and left to stir for 30 min. CQDs were formed by the dropwise addition of 6.0 mmol of the reducing agent over a period of 5 min. The solution was then left to stir for 30 min. The excess reducing agent was then quenched with the addition of 50 mL methanol, upon which the dispersion became transparent. Chemically passivated CQDs were formed by the dropwise addition of 200 µL of 0.1 M H_2PtCl_6 in isopropyl alcohol to the reaction vessel, followed by 3 mL (40.0 mmol) of allylamine. After stirring for 30 min, the reaction vessel was removed from the glove box and the organic solvent removed by rotary evaporation. The resulting dry powder (consisting mainly of surfactant) was then redispersed in 50 mL deionised water and sonicated for 30 min. The solution was then filtered twice using PVDF membrane filters (MILLEX-HV, Millipore, 0.45 µm) to remove the surfactant.

Characterisation

Transmission electron microscopy (TEM) images and selective area electron diffraction patterns (SAED) were acquired using a high-resolution JEOL 2100 electron microscope, equipped with a LaB_6 electron source and a Gatan DualVision 600 Charge-Coupled Device (CCD), operating at an accelerating voltage of 200 keV. TEM samples were prepared by depositing 100 µL of CQDs dispersion, onto a holey carbon coated TEM grid (400-mesh, #S147-3H, Agar Scientific). Particle size analysis of TEM images was carried out using the Particle Size Analzyer macro (r12, available online at http://code.google.com/p/psa-macro/), running on

Image J software. FT-IR spectra were recorded using a liquid cell with CaF_2 windows on a Perkin Elmer Two spectrometer. Samples were formed by placing an aliquot of carbon crystals dispersed in Chloroform onto CaF_2 plates, after which the sample was allowed to evaporate to dryness. X-ray photoelectron spectroscopy (XPS) measurements were carried out using a Kratos Ultra DLD photoelectron spectrometer. The narrow scan spectra were obtained under high vacuum conditions by using a monochromatic Al Kα x-ray radiation at 15 kV and 10 mA with an analyser pass energy of 20 eV. Substrates were cleaned for 20 min in piranha solution, rinsed with water and dried with nitrogen. A few drops of the CQD solution dissolved in chloroform were dropped on a clean gold surface substrate. All spectra were acquired at room temperature and binding energies were referenced to the Au $4f_{7/2}$ line. All spectra were fitted with three peaks using a Shirley background. UV-Vis absorption spectra were recorded using a Shimadzu UV PC-2401 spectrophotometer equipped with a 60 mm integrating sphere (ISR-240A, Shimadzu). Spectra were recorded at room temperature using a quartz cuvette (1 cm) and corrected for the solvent absorption.

Photoluminescence (PL) spectra of optically dilute solutions (optical density 0.01 - 0.1) were acquired on a Cary Eclipse luminescence spectrophotometer. Photoluminescence lifetime measurements were recorded on a scanning confocal fluorescence microscope (MicroTime 200, PicoQuant GmbH) equipped with a TimeHarp 200 TCSPC board. CQD samples were excited using a 402 nm pulsed diode laser (10 MHz; 70 ps pulse duration, LDH-P-C-400) that was spectrally filtered using a 405 nm band-pass filter (Z405/10x, Chroma Technology Corp.). A 50X objective (0.5 NA; LM Plan FL, Olympus Corp.) was used for focusing the excitation light onto the CQD dispersion and collecting the resultant fluorescence, which was directed onto an avalanche photodiode (APD; SPCM-AQR-14, Perkin-Elmer, Inc.). Backscattered excitation light was blocked with a 410 nm long-pass filter placed in the collection path (3RD410LP, Omega Optical). The excitation power was adjusted to maintain a count rate of $< 10^4$ counts/s at the APD in order to preserve single photon counting statistics. All emission lifetimes were fitted to a weighted multi-exponential model on FluoFit 4.2 software (PicoQuant GmbH). All lifetimes were fitted with a χ^2 value of less than 1.3.

Quantum yield measurements were carried out using the comparative method described by Williams *et al.*[28] Dilute dispersions of the CQDs in water were prepared with optical densities between 0.01 – 0.1 and compared against 9,10-diphenylanthracene (literature quantum yield of 90 % at 320 nm) as the standard.[29] Linear aggression analysis was employed to determine the relative PL intensities of the sample and references solutions over the range of concentrations. The quantum yield of the water soluble CQDs were recorded using the following equation:

$$\Phi_x = \Phi_R \left(\frac{m_x}{m_R} \right) \left(\frac{\eta_x^2}{\eta_R^2} \right)$$

where Φ is the quantum yield, m is the slope from the plot of integrated fluorescence intensity versus absorbance. The subscript R refers to the reference material of the known standard while x indicates the unknown species to be calculated.

Conclusions

In summary, allylamine-terminated carbon quantum dots have been synthesized using a simple, room–temperature microemulsion synthesis method, with well-defined core diameters controlled between 2 to 6 nm by varying the strength of the reducing agent. TEM imaging confirmed that the CQD are highly crystalline with a narrow size distribution, while the crystal structure was confirmed by selected area electron diffraction (SAED). FTIR and XPS spectroscopy confirmed that the CQDs possessed the same surface chemistry, with some evidence of surface oxidation. UV-Vis and PL spectroscopy show moderate absorption in the UV spectral range, and a strong blue emission with a marked dependency on excitation wavelength. Time resolved photoluminescence measurements showed lifetimes for all CQDs in the ns range, while determination of the photoluminescence quantum yield (Φ) of showed a maximum of 27% determined for 1.8 nm CQDs, comparable with the state of the art for room temperature synthesised nanocrystals. These water-soluble CQDs are highly photostable and resistant to aggregation, allowing their possible application in area including biological imaging and water-based ion sensing.

Acknowledgements

This work was supported by the European Commission under the FP7 Projects SNAPSUN (grant agreement n° 246310) and CommonSense (grant agreement n° 261809) and the Irish Higher Education Authority under the PRTLI program (cycle 3 “Nanoscience” and Cycle 4 “INSPIRE”).

Notes and references

Tyndall National Institute, University College Cork, Lee Maltings, Cork, Ireland. Email: hugh.doyle@tyndall.ie.

† Electronic Supplementary Information (ESI) available: Electronic Supplementary Information (ESI) available: Additional TEM images of the CQDs, photoluminescence spectra, quantum yield and fluorescence lifetime measurements. See DOI: 10.1039/b000000x/

1. H. Li, Z. Kang, Y. Liu and S. T. Lee, *J. Mater. Chem.*, 2012, 22, 24230-24253.
2. J. C. G. Esteves da Silva and H. M. R. Gonçalves, *TrAC, Trends Anal. Chem.*, 2011, 30, 1327-1336.
3. S. N. Baker and G. A. Baker, *Angew. Chem., Int. Ed.*, 2010, 49, 6726-6744.
4. Y. P. Sun, B. Zhou, Y. Lin, W. Wang, K. A. S. Fernando, P. Pathak, M. J. Meziani, B. A. Harruff, X. Wang, H. Wang, P. G. Luo, H. Yang, M. E. Kose, B. Chen, L. M. Veca and S. Y. Xie, *J. Am. Chem. Soc.*, 2006, 128, 7756-7757.

5. Q.-L. Zhao, Z.-L. Zhang, B.-H. Huang, J. Peng, M. Zhang and D.-W. Pang, *Chem. Commun*., 2008, 5116-5118.
6. H. Peng and J. Travas-Sejdic, *Chem. Mater*., 2009, 21, 5563-5565.
7. K. Linehan and H. Doyle, *RSC Adv.*, 2014, 4, 12094-12097.
8. S. K. Bhunia, A. Saha, A. R. Maity, S. C. Ray and N. R. Jana, *Sci. Rep.*, 2013, 3, art. no 1473.
9. X. Xu, R. Ray, Y. Gu, H. J. Ploehn, L. Gearheart, K. Raker and W. A. Scrivens, *J. Am. Chem. Soc.*, 2004, 126, 12736-12737.
10. H. Goncalves and J. C. G. Esteves da Silva, *J. Fluoresc.*, 2010, 20, 1023-1028.
11. H. Jiang, F. Chen, M. G. Lagally and F. S. Denes, *Langmuir*, 2009, 26, 1991-1995.
12. Q. L. Zhao, Z. L. Zhang, B. H. Huang, J. Peng, M. Zhang and D. W. Pang, *Chem. Commun*., 2008, 5116-5118.
13. L. Zheng, Y. Chi, Y. Dong, J. Lin and B. Wang, *J. Am. Chem. Soc*., 2009, 131, 4564-4565.
14. J. Zhou, C. Booker, R. Li, X. Zhou, T. K. Sham, X. Sun and Z. Ding, *J. Am. Chem. Soc.*, 2007, 129, 744-745.
15. H. Liu, T. Ye and C. Mao, *Angew. Chem., Int. Ed.*, 2007, 119, 6593-6595.
16. X. Wang, L. Cao, F. Lu, M. J. Meziani, H. Li, G. Qi, B. Zhou, B. A. Harruff, F. Kermarrec and Y. P. Sun, *Chem. Commun.*, 2009, 3774-3776.
17. D. Pan, J. Zhang, Z. Li, C. Wu, X. Yan and M. Wu, *Chem. Commun.*, 2010, 46, 3681-3683.
18. R. Liu, D. Wu, S. Liu, K. Koynov, W. Knoll and Q. Li, *Angew. Chem., Int. Ed.*, 2009, 121, 4668-4671.
19. J. Zong, Y. Zhu, X. Yang, J. Shen and C. Li, *Chem. Commun.*, 2011, 47, 764-766.
20. A. B. Bourlinos, A. Stassinopoulos, D. Anglos, R. Zboril, V. Georgakilas and E. P. Giannelis, *Chem. Mater.*, 2008, 20, 4539-4541.
21. H. Zhu, X. Wang, Y. Li, Z. Wang, F. Yang and X. Yang, *Chem. Commun.*, 2009, 5118-5120.
22. X. Wang, K. Qu, B. Xu, J. Ren and X. Qu, *J. Mater. Chem*., 2011, 21, 2445-2450.
23. H. Li, X. He, Z. Kang, H. Huang, Y. Liu, J. Liu, S. Lian, C. H. A. Tsang, X. Yang and S.-T. Lee, *Angew. Chem., Int. Ed.*, 2010, 49, 4430-4434.
24. W. Kwon and S. W. Rhee, *Chem. Commun.*, 2012, 48, 5256-5258.
25. W. Kwon, G. Lee, S. Do, T. Joo and S.-W. Rhee, *Small*, 2014, 10, 506-513.
26. K. Linehan and H. Doyle, *RSC Adv.*, 2014, 4, 18-21.
27. K. Linehan and H. Doyle, *Small*, 2014, 10, 584–590.
28. A. T. R. Williams, S. A. Winfield and J. N. Miller, *Analyst*, 1983, 108, 1067-1071.
29. S. Hamai and F. Hirayama, *J. Phys. Chem.*, 1983, 87, 83-89.